Eng. Sci., 2022, **20**, 180–187

Engineered Science

DOI: https://dx.doi.org/10.30919/es8d695

Hysteresis-Free and Efficient Perovskite Solar Cells Using Stannic Oxide with Self-assembly L-Cysteine Layer

Putao Zhang, Shenghan Wu, Yiming Chen, Xiaohui Li, Fuhao Sun, Meiyue Liu, Zeng Chen and Shengjun Li*

Abstract

Perovskite solar cells (PSCs) with stannic oxide (SnO_2) electron transport layer (ETL) still face the challenge of low efficiency with serious hysteresis due to the nonradiative recombination at the SnO_2/perovskite interface. Herein, a self-assembly modification layer with multifunctional properties using L-Cysteine (Cys) is applied to solve the above issues. Through applying this novel self-monolayer between SnO_2 and perovskite film, the trap state is greatly alleviated as well with an enhanced charge extraction. In addition, the naked -NH_2 and sulfur atom of this monolayer will affect the crystallization dynamics of perovskite film, resulting in an improved film quality. Compared with the control device with a power conversion efficiency (PCE) of 18.55%, the monolayer contacts engineered device shows a significantly increase PCE over 21% along with negligible hysteresis. More interestingly, monolayer contacts engineered PSCs exhibit superior stability that over 90% of its initial PCE remains after stored at 50% relative humidity for 50 days. This work provides a promising method to fabricate planar n-i-p perovskite devices with high efficiency, stability, and repeatability.

Keywords: Perovskite solar cells; Electron transport layer; Hysteresis; Stability; Interface.
Received: 16 March 2022; Revised: 04 April 2022; Accepted: 14 April 2022.
Article type: Research article.

1. Introduction

Organic-inorganic metal halide perovskite solar cells (PSCs) have attracted worldwide attention due to their excellent photoelectric properties and low manufacturing costs. Owing to the continuous optimization of the perovskite composition, film quality and device structure, the certified efficiency has increased from 3.8% to 25.7% in just over a decade.[1,2] However, PSC is still affected by non-radiative loss from interface or bulk trap state.[3,4] It is considered that interface carrier recombination is one of the main factors of energy loss.[5] The interface energy loss caused by energy level mismatch, non-ideal contact and interface defects will cause massive charge accumulation, which will lead to the degradation of device performance.[6-9] In addition, the serious current-voltage (*J-V*) hysteresis and poor device stability are also related to energy level mismatch and carrier recombination at the interface. Therefore, improving charge extraction at the interface is crucial to minimize energy loss and improve the device performance.

In order to reduce the interface defects, many interface modification strategies have been proposed, such as fullerene and their derivatives, carbon quantum dots and lithium salts are used for doping or surface modification.[10-16] In addition, Wang et al. reported that RbF can be mixed into stannic oxide (SnO_2) colloidal dispersion as an additive. The F-Sn bond changes the electron cloud density around Sn and improves the electron mobility of SnO_2. This reduces voltage loss, at the same time, eliminates the hysteresis phenomenon.[17] Facchetti and his co-workers have reported that SnO_2 electron transport layer (ETL) modified by non-conjugated small-molecule zwitterion electrolyte not only passivates the SnO_2/perovskite interface, but also passivates the defects of perovskite from bottom to top. The benefit of this is further improving charge separation, increasing open circuit voltage and suppressing hysteresis phenomenon.[18] These results indicate that doping and interface modification are effective strategies for passivating SnO_2/perovskite interface defects and accelerating charge transport to obtain high performance PSCs.

In this work, we introduced Cys onto SnO_2 surface and studied its impact on photovoltaic property of PSCs. There are three reasons for choosing Cys as a passivation material: Firstly, the passivation molecule can firmly combine with ETL. Here, Cys molecule firmly anchored on the SnO surface by forming new bond (condensation of -COOH in Cys and -OH on SnO_2). Secondly, -NH_2 in Cys can induce the perovskite crystallization and promote the formation of large grains.

Key Laboratory of Photovoltaic Materials, Henan University, Kaifeng, Henan, 475004, China.
**E-mail:*lishengjun@henu.edu.cn (S. Li)

Thirdly, the passivation layer increases surface wettability of SnO_2 film. Previous studies have shown that, the more hydrophilicity of ETL, the lower Gibbs free energy (G) of heterogeneous nucleation, which makes it easier to get perovskite films with big grain.[19] Therefore, the highest power conversion efficiency (PCE) of PSC with structure of ITO/SnO_2-Cys/Perovskite/Spiro-OMeTAD/Au reached PCE of 21.07%, which is significantly higher than that of control devices (18.55%). The stability of the passivated devices has also significantly improved and the details will be discussed in the following sections.

2. Results and discussions

Molecular structure of Cys as shown in Fig. 1a, containing a carboxyl group (-COOH), a sulfur atom (S) and an amino group ($-NH_2$). These chemical group let Cys a potential candidate for interface modification of SnO_2 ETL. The -COOH can condense with -OH of SnO_2 surface to block the polar group (Fig. 1a). The $-NH_2$/S can form adducts with negatively/positively charged trapped states to passivate surface traps of perovskite. Surface electrostatic potential of Cys is analyzed by density functional theory (DFT) method, as shown in Fig. 1a, S/$-NH_2$ lays in negative/positive potential region, which can coordinate with uncoordinated Pb^{2+} or halogen. The strong electron donating group on Cys is helpful to enhance the electron density in the negative potential region, and can significantly improve the reactivity of C=O group in Cys. As crystal growing substrate, ETL has important effect on perovskite crystallinity and morphology. We further investigated the influence of Cys monolayer on perovskite films. Mixed cationic perovskite was prepared on different ETLs by one-step spin-coating method (chlorobenzene as anti-solvent), the process as shown in Fig. 1b. Details for perovskite fabrication are provided in the experimential section (Supportting Information). The Cys assisted crystallization process as shown in Fig. 1b. Cys is strongly anchored on the SnO_2 surface through Sn-O-C bonds to form both an effective barrier to reduce the damage of perovskite by polar groups on the SnO_2 surface, and form a bridge between perovskite and ETL to realize effective charge transfer. Furthermore, the S atoms and $-NH_2$ in Cys combine with Pb^{2+} or other negative/positively charged trap states, forming a Lewis adduct to passivate surface defects. Therefore, perovskite crystallization rate reduced, and high-quality thin film with big grain were prepared. Notably, the grain size of control is much smaller than that of perovskite on SnO_2-Cys, and this is proposed to be caused by the monolayer of Cys on surface of SnO_2, which will be further confirmed and discussed in the next section.

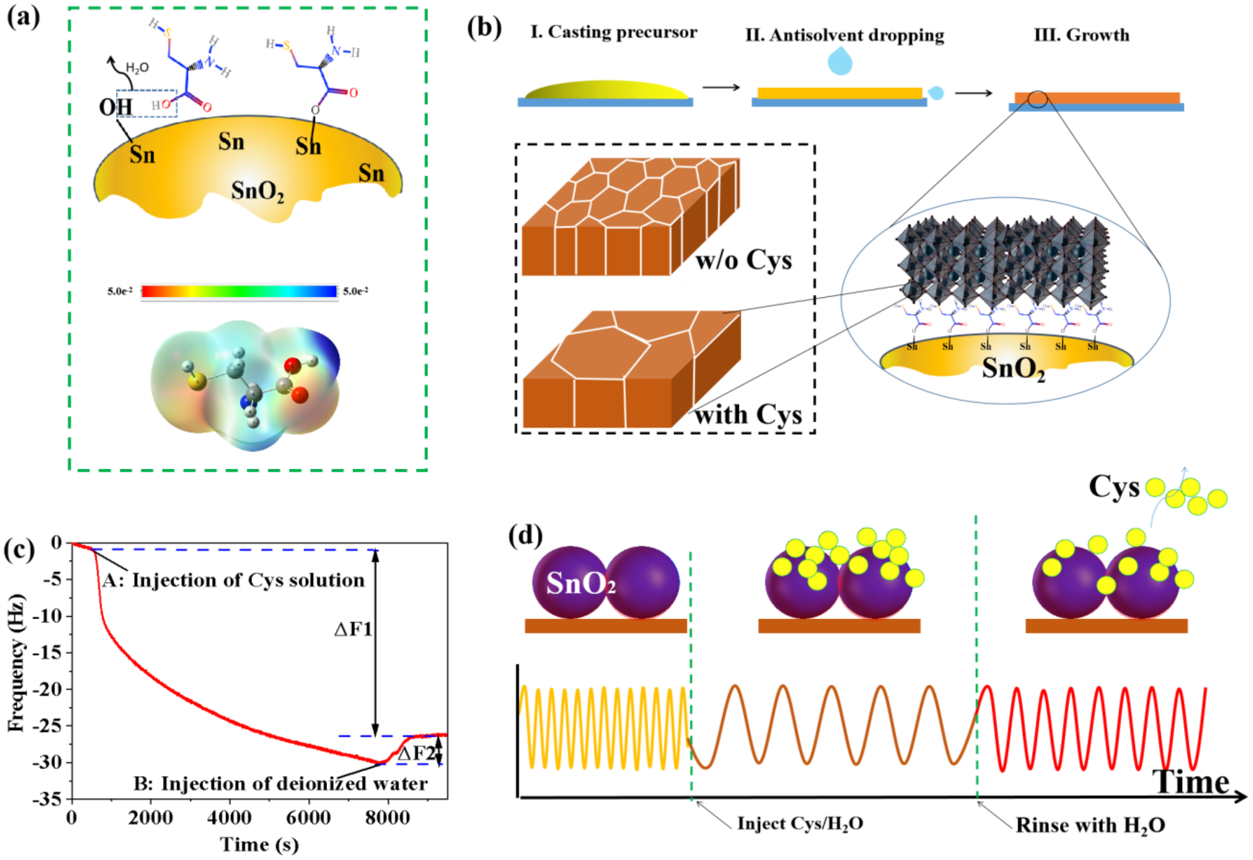

Fig. 1 (a) Molecular model and schematic diagram of Cys binding on the SnO_2 surface (Top), electrostatic potential profile of Cys(bottom). (b) Illustration of perovskite preparation process and crystals growth induced by the interfacial Cys. (c) Monitoring the adsorption of Cys on SnO_2 by quartz crystal microbalance. (d) Schematic diagram of vibration frequency variation of quartz crystal microbalance.

To investigate the process of Cys adsorption on SnO_2, the binding of Cys molecules on SnO_2 was monitored by quartz crystal microbalance (QCM) in real time. The results are shown in Fig. 1c. The process is that Cys was injected into SnO_2 layer at a point A, which results in a rapid decrease in the vibration frequency until equilibrium is achieved (See Fig. 1d). In this process, with injection time increase, the vibration frequency becomes lower, while frequency decreasing speed becomes slower, which indicates that Cys molecules gradually reach adsorption/desorption equilibrium at the solid-liquid interface. It should be noted that the equilibrium at this time is dynamic equilibrium. If Cys solution is stopped or replaced by other solution, the equilibrium will be broken. When deionized water injected at point B (Fig. 1c), the original equilibrium is broken, and the weakly bound Cys molecules are washed away. During the rinsing process, parts of weakly bound Cys desorb from SnO_2. Therefore, at point B, the vibration frequency rises again, finally tends to be stable. Vibration frequency variation ΔF1 and ΔF2 represent strongly/chemically and weakly/physically bound Cys, respectively. In order to more intuitively observe the adsorption of Cys on SnO_2, the change of SnO_2 during adsorption/rinsing process were calculated by Sauerbrey formula.[20,21] As shown in Fig. S1, the mass of SnO_2 changes with the increase of adsorption/rinsing time. The mass change of SnO_2 with different Cys concentrations as shown in Fig. S2. As shown in Fig. S2, increasing the concentration of Cys (0.5 to 1.0 mM), the equilibrium adsorption capacity also increases. Equilibrium adsorption capacity remained unchanged when the concentration increased continuously (1.0 to 2.0 mM). Therefore, 1.0 mM Cys is enough to make a saturation adsorption of the SnO_2 surface. The results of QCM proved that Cys can strongly adsorb on SnO_2. We believe that SnO_2 surface contains hydroxyl (-OH) and carboxyl groups (-COOH), which can bind to the Cys molecules.

The binding of Cys and SnO_2 was confirmed by fourier transform infrared (FTIR) spectroscopy. In Fig. 2a, a strong peak locate at 3410 cm^{-1} assigned to characteristic peak of O-H bond. FTIR spectra for Cys in Fig. S3 shows a characteristic peak at 1670 cm^{-1}, which belongs to C=O (stretching vibration). After Cys combined on SnO_2, C=O peak value shift significantly to lower wave number (1654 cm^{-1}), indicating that SnO_2 (-OH) interacted with Cys ($-COO^-$). In addition, as shown in Fig. S4, the change of contact angle before and after treatment is very obvious (from 25.1° down to 16.2°), which further confirms the existence of hydrophilic molecules, Cys, on SnO_2 surface. Small contact angle indicates that the surface hydrophilicity of SnO_2 is improved upon Cys treatment. This decreases nucleation free energy, which is helpful in obtaining compact and flat perovskite films.[19,22] In order to observe the morphology change of SnO_2 caused by Cys passivation layer, the surface was studied by AFM, results are shown in Fig. S5. In comparison of the control, SnO_2-Cys is smoother with a R_q of 1.32 nm (Control group, R_q= 2.87 nm), which is instrumental in growth high quality perovskite grains.[23,24] The preparation process of Cys passivation layer in detail is shown in the experimental section (Supporting Information). SnO_2 thin films were immersed in aqueous solution containing Cys molecules for 30 min and then rinsed with ultra-pure water, followed by the baking at 100 ℃ for 0.5 h. As shown in Fig. 2b, Cys was anchored on SnO_2 surface by carboxylic group (-COOH). It is worth noting that the sulfur atoms, amino groups and carboxyl groups exposed on the surface of SnO_2-Cys play a positive role in crystallization process of perovskite owing to the lewis acid-base interaction between these functional groups and undercoordinated Pb and the other negative/positively charged trap states.[25]

First principle calculation was carried out to deeply understand the atomic structure of SnO_2-Cys/CsFAMA interface. In order to simplify the calculation, atomic ratio (FA/MA and I/Br) in perovskite crystals have been treated approximately. Considering the small content of Cs, Cs atoms are not included in the model. Fig. 2c shows a strong interaction between S of Cys and Pb of CsFAMA to form Pb-S bond. This interaction does not significantly change the structure of perovskite crystal. More importantly, Pb-S bond can effectively reduce the formation of deep level traps of perovskite and improve the chemical stability of it. As shown in Fig. S6, the SnO_2/CsFAMA film placed in the dark air for 50 days decomposes seriously, while the SnO_2-Cys/CsFAMA film decomposes slightly (Temperature ≈ 25 ℃, Relative Humidity≈50%).

The XPS spectra of SnO_2 and SnO_2-Cys films are shown in Fig. 2d. To eliminate surface charge, silicon substrates were grounded through silver paste. After washing with deionized water, the peak corresponding to N, S elements still exist (Fig. 2d and Table S1), which indicates that Cys is successfully bound to the SnO_2 surface. This is consistent with QCM and FTIR. In addition, in high resolution XPS, the peak positions of Sn 3d and O 1s were shifted after Cys modification (Fig. S7), which further proved that Cys molecules were bound to SnO_2. Energy dispersive spectrometry (EDS) (Fig. S8) also proved existence of S, N on SnO_2-Cys film. The transmission spectra of ITO/SnO_2 and ITO/SnO_2-Cys as shown in Fig. 2e. These samples show a good transmittance in the visible region (400~800 nm). Transmittance of the SnO_2-Cys has no significant decrease, indicating that the absorption loss of the passivation layer of Cys can be ignored. Therefore, both SnO_2 and SnO_2-Cys films are expected to have a good optical quality. The effect of Cys on energy levels of SnO_2 was further analyzed by UV-vis absorption and XPS measurements (Fig. S9). The minimum conduction band (CBM) of bare SnO_2 is 7.75 eV, while the CBM of SnO_2-Cys can be adjusted to 7.71 eV, which is more closer to the CBM of perovskite layer. The matched energy levels between SnO_2-Cys and perovskite can promote the effective charge transfer at interface, reducing the charge accumulation and carrier recombination.

Electron mobility is an important index to evaluate ETL in PSCs. The electron-only device fitted with the Mott-Gurney law was used to evaluate electron mobility (μ_e) of ETL films.[26]

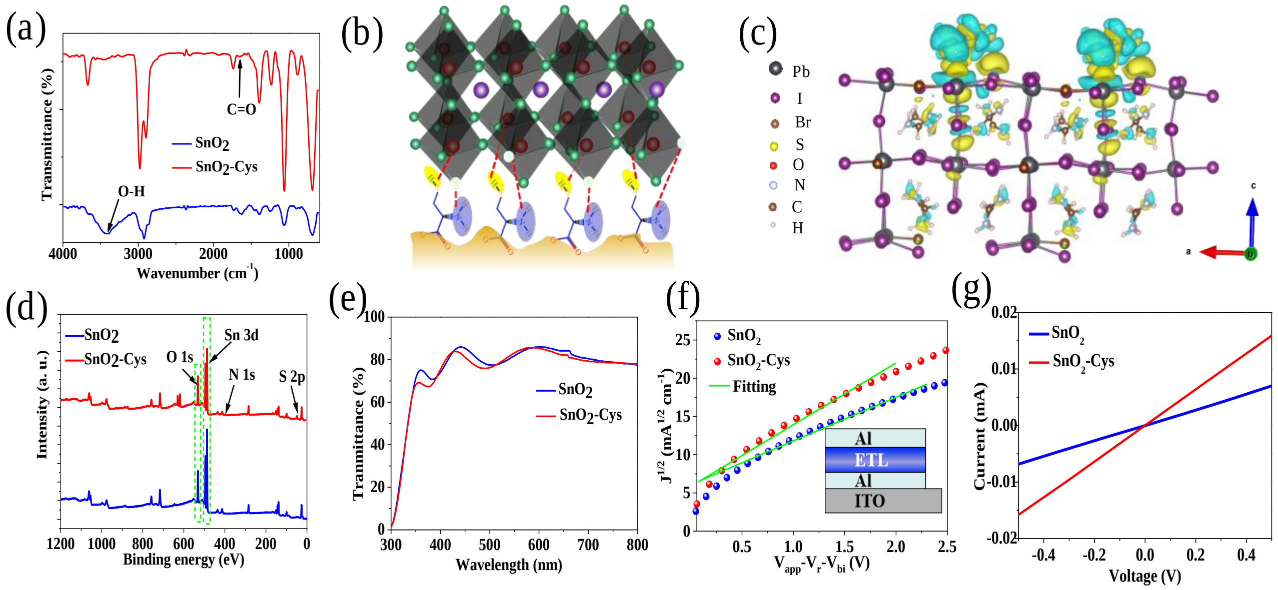

Fig. 2 (a) FTIR spectra of SnO_2 and SnO_2-Cys films. (b) Schematic illustration of Cys at the interface between SnO_2 and perovskite. (c)Interfacial bonding interaction at the SnO_2/CsFAMA interface.(d) XPS spectra of ETLs, for which the peaks of Sn 3d, N 1s, O 1s, S 2p are marked. (e) Optical transmission spectra of ITO/SnO_2 and ITO/SnO_2-Cys samples. (f) Electron mobility of SnO_2 and SnO_2-Cys films (device structure: ITO/Al/ETL/Al). (g) J-V curvesfor evaluating the conductivity of SnO_2 and SnO_2-Cys films (devices structure: ITO/ETL/Al).

As shown in Fig. 2f, the μ_e of SnO_2 or SnO_2-Cys films can be obtained by the Equation (1). The electron mobility of SnO_2-Cys is 1.42×10^{-3} $cm^2v^{-1}s^{-1}$, which is significantly larger than that of control (7.09×10^{-4} $cm^2v^{-1}s^{-1}$).

$$\mu_e = \frac{8JL^3}{9\varepsilon_0\varepsilon(V_{app}-V_r-V_{bi})^2} \qquad (1)$$

where L is the thickness of SnO_2 or SnO_2-Cys films, ε_0 and ε are the vacuum permittivity and relative dielectric constant, V_{app}, V_{r}, and V_{bi} are the applied voltage, the voltage drop and the built in voltage (compared with V_{app}, V_r and V_{bi} are very small and negligible), J and μ_e are current density and electron mobility. The increase of μ_{e} indicates that introduction of Cys can effectively promote the electron transport of the ETL, which is conducive to charge transport in PSCs. We fabricated a device with structure of ITO/ETL/Al to measure the conductivity difference of ETLs. Fig. 2g show that the conductivity of SnO_2-Cys increases significantly. The significant increase of conductivity in the ETL does promote the carrier transport in devices, reduce interface carrier accumulation, thus improving the performance and suppressing the hysteresis.

Quality of photoactive layers, including perovskite grain size, film crystallinity, and the surface coverage, is a very important factor affecting properties of PSCs. The SEM images of the mixed-cation perovskite spin-coated on different ETLs are shown in Figs. 3a-b. It is obvious that both films with disorderly connected grains, are pin-hole free, smooth and compact. However, most of the grains on SnO_2-Cys are obviously larger than those on SnO_2. The histogram of grain size is shown in Fig. S10. Grain size of perovskite on the SnO_2-Cys and SnO_2 films are about 700 and 420 nm in average, respectively. AFM images of perovskite films on SnO_2-Cys (Fig. S11) also show smaller root mean square (RMS) values and larger domains than those on SnO_2, demonstrating that surface defects and the surface potential fluctuations of SnO_2-Cys are reduced.[27] In the Fig. S12, the contact angle of perovskite precursor solution dripped on SnO_2-Cys is ≈ 5.1° which is smaller than that on SnO_2 (≈7.1°). This indicates that SnO_2-Cys thin films rich in amino and sulfur atoms have smaller surface energy and better interfacial wettability for the perovskite precursors. It is well known that the lower Gibbs free energy in heterogeneous nucleation contributes to the nucleation of perovskite.[28,29] Therefore, the monolayer, Cys, rich in amino and carboxyl groups on SnO_2-Cys can increase perovskite grain size and crystallinity, as shown in SEM and AFM results. The coordination bond slows down crystallization rate and promotes the formation of large grains. The UV-Vis absorption results of perovskite are shown in Fig. 3c. The increased absorption of SnO_2-Cys/perovskite can be attributed to big grains caused by Cys monolayer. XRD patters of the perovskite films in Fig. S13 show the characteristic diffraction peaks of perovskite phase. Compared with SnO_2/perovskite film, the enhanced diffraction peak intensities of SnO_2-Cys/perovskite, indicating that Cys contributes to the improved crystallinity of perovskite.[30] The effect of Cys on the charge recombination dynamics between ETL and perovskite were further investigated by steady state photoluminescence and time-resolved photoluminescence.

Photoquenching of perovskite films grown on SnO_2-Cys is more effective than that on bare SnO_2, as shown in Fig. 3d, which indicates that the Cys passivation layer enhances electron extraction and reduces charge recombination.

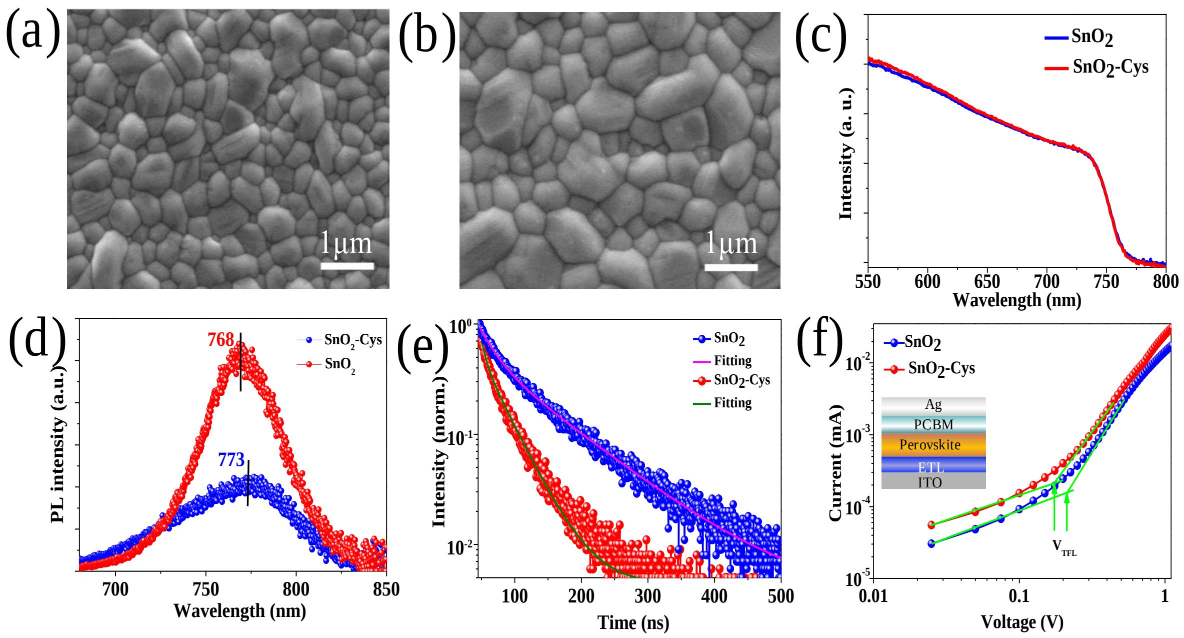

Fig. 3 SEM images of (a) SnO_2/perovskite and (b) SnO_2-Cys/perovskite. Absorption spectrum (c), steady state photoluminescence (d) and time-resolved photoluminescence (e) spectra of perovskite films. (f) *I-V* curves with V_{TFL} kink points (measured in dark). The electron-only device structure shows in inset.

Compared with the control, PL peak of SnO_2-Cys/perovskite films showed a blue shift of 5 nm, indicating that the defect sites were passivated by lewis acid-base reaction. The TRPL shows in Fig. 3e, which is fitted with the functions Equation (2), fitting results are shown in Table S2.

$$f(t) = A_1\, exp(-\frac{t}{\tau_1}) + A_2 \exp(-\frac{t}{\tau_2}) + \gamma_0 \qquad (2)$$

The τ_1 and τ_2 are ascribed to the charge transfer at interface (ETL/perovskite) and charge radiative recombination in perovskite film, respectively.[31] Shortening of τ_1 (from 15.36 to 4.26 ns) indicates faster carrier extraction charge from perovskite to Cys-SnO_2 ETL. This can be attributed to the more matched energy levels between SnO_2-Cys ETL and perovskite (Fig. S14). The slow decay lifetime τ_2 increases for SnO_2-Cys/perovskite (from 64.75 to 114.32 ns) indicates Cys monolayer reduces recombination rate in bulk perovskite. The main reason for decrease of nonradioactive recombination is the large grain size and less grain boundary. High quality perovskite films suggest low trap density and excellent photoelectric properties. To estimate trap density in bulk perovskite, SCLC was applied to electron-only devices (ITO/ETL/perovskite/PCBM/Ag) to quantitative obtain n_t of perovskite films on different ETL. The device shows a linear relationship under low bias, as shown in Fig. 3f. With the increase of bias, traps are filled continuously, and the current injection increases significantly until V_{TFL} is reached. The n_t is calculated by Equation (3).[32,33]

$$n_t = \frac{2\varepsilon\varepsilon_0 V_{TFL}}{eL^2} \qquad (3)$$

where e, $\varepsilon/\varepsilon_0$ and L are the electron charge number, vacuum/relative permittivity and perovskite film thickness, respectively. The n_t are calculated to be 3.7×10^{15} and 2.9×10^{15} cm^{-3} for SnO_2 and SnO_2-Cys samples, respectively. We further compared the Urbach energy (E_U) of perovskite films, which provides important information about the disorder of shallow level electrons.[34-36] The results are shown in Fig. S15. Compared with control, E_U value of the SnO_2-Cys sample is smaller, which indicates that trap density based on the SnO_2-Cys is lower, which is consistent with the above calculation results and TRPL results. Dark current of SnO_2-Cys based devices is lower than that of control (Fig. S16), which further confirms that perovskite grown on SnO_2-Cys has lower trap density.

In order to determine how Cys enhance the performance of PSCs, we have prepared a series of mix-cation PSCs based on different ETLs. As shown in Fig. 4a, device with architecture of ITO/ETL/perovskite/Spiro-OMeTAD/Au. The photovoltaic parameters of 40 independent devices for SnO_2-Cys and control are shown in Fig. S17, after passivation, the voltage distribution of the device more narrower. The increase of V_{OC} and FF leads to the improvement of PCE. The cross-sectional SEM image of the device is shown in Fig. 4b. It can be seen from the thickness of each layer that perovskite grains big enough to go through the whole film. Fig. 4c shows *J-V* curves of champion cells under one standard simulated sunlight. The device based on SnO_2 reaches a highest efficiency of 18.55% with a V_{oc} of 1.08 V, a J_{sc} of 21.97 mA cm^{-2}, and a *FF* of 77.6% from the reverse scan. When Cys is introduced on the SnO_2, V_{oc}, J_{sc}, and *FF* are increased to 1.15 V, 23.26 mA cm^{-2}, and 78.51%, respectively, reaching a PCE of 21.07%. Fig. 4d shows the IPCE spectrum. Integral J_{SC} of control and SnO_2-Cys based device are 20.13 and 21.52 mA cm^{-2}, respectively, which is very consistent with J_{SC} value measured by *J-V*. It has been reported that the hysteresis phenomenon may be caused

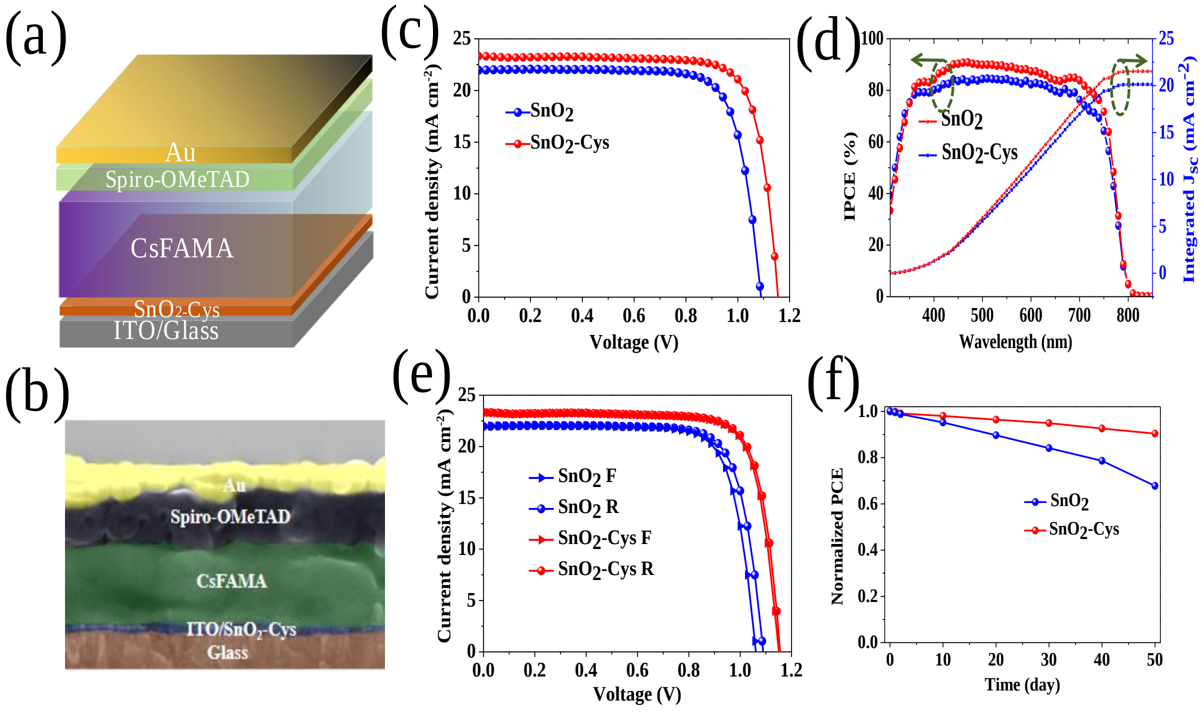

Fig. 4 (a) Structure diagram of mixed-cation PSCs. (b) The cross-sectional SEM image of planar PSCs. (c) *J-V* curves of champion solar cells. (d) IPCE curves and integrated current density of the two devices. (e) *J-V* curves of forward and reverse scans. (f) Stability of PSCs based on the SnO_2 and SnO_2-Cys.

by charge/ion carriers, ion trap state migration and trap density. *J-V* hysteresis is usually evaluated by hysteresis index ($HI=PCE_{reverse}-PCE_{forward})/PCE_{reverse}$). HI of SnO_2 and SnO_2-Cys based devices are 3.36% and 0.64%, respectively (Fig. 4e). Therefore, the devices assembled by SnO_2-Cys exhibit small hysteresis, indicating a substantially reduced trap-assisted recombination, which could be attributed to a larger grain size and lower trap density, leading to efficient charge extraction and corresponding suppressed charge recombination.[37,38] This observation was also verified by the results of electrochemical impedance spectroscopy (EIS) measurements, for which SnO_2-Cys-based device possessed a large recombination resistance (Fig. S18 and Table S3), indicating that Cys nomolayer reduces interfacial carrier recombination. Transient photovoltage (TPV) is an important technique to study carrier lifetime and carrier recombination dynamics.[39,40] We measured the TPV decay to characterize the charge lifetime of the control and SnO_2-Cys based devices (Fig. S19). The TPV decay lifetimes of the SnO_2-Cys based device (12.3 μs) is much longer than the control (6.29 μs for the SnO_2 based device). The longer lifetime indicates that the process of interfacial charge recombination is slowed down for the SnO_2-Cys based PSC, which is consistent with the PL and TRPL results. As discussed above, Cys nomolayer not only induces the formation of big grains, but also improves the efficiency of PSCs. The reduction of grain boundary and interface defects can prevent the invasion of water and samples, and then enhance the stability of the film. For solar cell device, stability is also a key indicator for commercial application. Therefore, the stability test is conducted to observe the long-term stability of the devices in air conditions. Fig. 4f shows the relationship between normalized PCE and storage time. The device based on SnO_2-Cys maintains 90% of its initial efficiency even after 50 days in an ambient dark atmosphere (T≈25℃, H≈50%) . On the other hand, the control device only maintains 68% of its initial efficiency under the same storage condition.

3. Conclusions

In conclusion, we propose an effective passivation method to change the electronic properties of SnO_2 ETL and passivate the interface of ETL/perovskite. Cys molecule is firmly anchored onto the SnO_2 surface by Sn-O-C bond. The exposed $-NH_2$ and S of Cys induces the formation of big grain perovskite. Higher electron mobility and lower electron trap in the passivated SnO_2 ETL improve the electron extraction rate and reduce interface carrier recombination. At the same time, perovskite with big grain exhibits excellent optical absorption and less grain boundary density. The champion PCE as high as 21.07%, and the device maintains 90% of its initial performance in the atmospheric environment after 50 days. The application of SnO_2 surface passivation engineering in plane *n-i-p* devices is an effective way to enhance the performance and long-term stability of PSCs.

Acknowledgements

This work was supported by Natural Science Foundation of Henan Province (No. 202300410073) and China Postdoctoral Science Foundation (2021M690907).

Conflict of Interest

The authors declare no conflict of interest.

Supporting information

Applicable.

Reference

[1] A. Kojima, K. Teshima, Y. Shirai, T. Miyasaka, Organometal halide perovskites as visible-light sensitizers for photovoltaic cells, *Journal of the American Chemical Society*, 2009, **131**, 6050-6051, doi: 10.1021/ja809598r.

[2] Z. Xu, X. Zhou, X. Li, P. Zhang, Polymer-regulated SnO_2 composites electron transport layer for high-efficiency n-i-p perovskite solar cells, *Solar RRL*, 2022, **6**, 2200092, doi: 10.1002/solr.202200092.

[3] C.-L. Mai, Q. Zhou, Q. Xiong, C.-C. Chen, J. Xu, Z. Zhang, H.-W. Lee, C.-Y. Yeh, P. Gao, Donor-π-acceptor type porphyrin derivatives assisted defect passivation for efficient hybrid perovskite solar cells, *Advanced Functional Materials*, 2021, **31**, 2007762, doi: 10.1002/adfm.202007762.

[4] P. Zhang, Y. Chen, S. Wu, X. Li, M. Liu, S. Li, Enhancing the performance of n-i-p perovskite solar cells by introducing hydroxyethylpiperazine ethane sulfonic acid for interfacial adjustment, *Nanoscale*, 2022, **14**, 35-41, doi: 10.1039/d1nr05939d.

[5] K. Schutt, P. K. Nayak, A. J. Ramadan, B. Wenger, Y.-H. Lin, H. J. Snaith, Overcoming zinc oxide interface instability with a methylammonium-free perovskite for high-performance solar cells, *Advanced Functional Materials*, 2019, **29**, 1900466, doi: 10.1002/adfm.201900466.

[7] X. Li, S. Wu, Y. Chen, J. Tang, M. Liu, Z. Chen, P. Zhang, S. Li, Grain boundary defect controlling of perovskite via N-hydroxysuccinimide post-treatment process in efficient and stable n-i-p perovskite solar cells, *Solar RRL*, 2022, **6**, 2200502, doi: 10.1002/solr.202200502.

[8] H. Wang, F. Zhang, Z. Li, J. Zhang, J. Lian, J. Song, J. Qu, W.-Y. Wong, Naphthalene imide dimer as interface engineering material: an efficient strategy for achieving high-performance perovskite solar cells, *Chemical Engineering Journal*, 2020, **395**, 125062, doi: 10.1016/j.cej.2020.125062.

[9] Y. Chen, S. Wu, X. Li, M. Liu, Z. Chen, P. Zhang, S. Li, Efficient and stable low-cost perovskite solar cells enabled by using surface passivated carbon as the counter electrode, *Journal of Materials Chemistry C*, 2022, **10**, 1270-1275, doi: 10.1039/d1tc05351e.

[11] S. You, H. Wang, S. Bi, J. Zhou, L. Qin, X. Qiu, Z. Zhao, Y. Xu, Y. Zhang, X. Shi, H. Zhou, Z. Tang, A biopolymer heparin sodium interlayer anchoring TiO_2 and $MAPbI_3$ enhances trap passivation and device stability in perovskite solar cells, *Advanced Materials*, 2018, **30**, 1706924, doi: 10.1002/adma.201706924.

[12] N. Tsvetkov, M. E. Khan, B. C. Moon, Y.-H. Kim, J. K. Kang, Strain-induced metallization and defect suppression at zipper-like interdigitated atomically thin interfaces enabling high-efficiency halide perovskite solar cells, *ACS Nano*, 2021, **15**, 1805-1816, doi: 10.1021/acsnano.0c09584.

[13] H. Wang, F. Yang, N. Li, J. Song, J. Qu, S. Hayase, W.-Y. Wong, Interface engineering with a novel n-type small organic molecule for efficient inverted perovskite solar cells, *Chemical Engineering Journal*, 2020, **392**, 123677, doi: 10.1016/j.cej.2019.123677.

[14] C. H. Li, M. J. Feng, F. Guo, Q. L. Jiang, N. Li, Z. H. Guo, X.H. Liu, The Evolution of Tin-Based Perovskites Solar Cells, *Engineered Science*, 2022, **19**, 1-4, doi: 10.30919/es8d638.

[15] H. Wang, Y. Guo, L. He, L. Kloo, J. Song, J. Qu, P.-C. Qian, W.-Y. Wong, Efficient naphthalene imide-based interface engineering materials for enhancing perovskite photovoltaic performance and stability, *ACS Applied Materials & Interfaces*, 2020, **12**, 42348-42356, doi: 10.1021/acsami.0c11620.

[16] C. J. Bhongale, R. Chaudhari, All-organic solution processed solar cells based on terephthaladehyde self-assembled monolayer, *Engineered Science*, 2021, **15**, 89-94, doi: 10.30919/es8d457.

[17] J. Zhuang, P. Mao, Y. Luan, N. Chen, X. Cao, G. Niu, F. Jia, F. Wang, S. Cao, J. Wang, Rubidium fluoride modified SnO_2 for planar n-i-p perovskite solar cells, *Advanced Functional Materials*, 2021, **31**, 2010385, doi: 10.1002/adfm.202010385.

[18] D. Zheng, R. Peng, G. Wang, J. L. Logsdon, B. Wang, X. Hu, Y. Chen, V. P. Dravid, M. R. Wasielewski, J. Yu, W. Huang, Z. Ge, T. J. Marks, A. Facchetti, Perovskite solar cells: simultaneous bottom-up interfacial and bulk defect passivation in highly efficient planar perovskite solar cells using nonconjugated small-molecule electrolytes, *Advanced Materials*, 2019, **31**, 1970283, doi: 10.1002/adma.201970283.

[19] D. Yang, R. Yang, K. Wang, C. Wu, X. Zhu, J. Feng, X. Ren, G. Fang, S. Priya, S. Liu, High efficiency planar-type perovskite solar cells with negligible hysteresis using EDTA-complexed SnO_2, *Nature Communications*, 2018, **9**, 3239, doi: 10.1038/s41467-018-05760-x.

[20] K. K. Kanazawa, G. G. Joseph, Frequency of a quartz microbalance in contact with liquid, *Analytical Chemistry*, 1985, **57**, 1770-1771, doi: 10.1021/ac00285a062.

[21] H. K. Wayment-Steele, L. E. Johnson, F. Tian, M. C. Dixon, L. Benz, M. S. Johal, Monitoring N3 dye adsorption and desorption on TiO_2 surfaces: a combined QCM-D and XPS study, *ACS Applied Materials & Interfaces*, 2014, **6**, 9093-9099, doi: 10.1021/am500920w.

[22] S. Zhao, K. Yamamoto, S. Iikubo, S. Hayase, T. Ma, First-principles study of electronic and optical properties of lead-free double perovskites Cs_2NaBX_6 (B = Sb, Bi; X = Cl, Br, I), *Journal of Physics and Chemistry of Solids*, 2018, **117**, 117-121, doi: 10.1016/j.jpcs.2018.02.032.

[23] C.-S. Jiang, M. Yang, Y. Zhou, B. To, S. U. Nanayakkara, J. M. Luther, W. Zhou, J. J. Berry, J. van de Lagemaat, N. P. Padture, K. Zhu, M. M. Al-Jassim, Carrier separation and transport in perovskite solar cells studied by nanometre-scale profiling of electrical potential, *Nature Communications*, 2015, **6**, 8397, doi: 10.1038/ncomms9397.

[24] X. Ren, D. Yang, Z. Yang, J. Feng, X. Zhu, J. Niu, Y. Liu, W. Zhao, S. F. Liu, Solution-processed Nb: SnO_2 electron transport layer for efficient planar perovskite solar cells, *ACS Applied*

Materials & Interfaces, 2017, **9**, 2421-2429, doi: 10.1021/acsami.6b13362.

[25] F. Zhang, K. Zhu, Additive engineering for efficient and stable perovskite solar cells, *Advanced Energy Materials*, 2020, **10**, 1902579, doi: 10.1002/aenm.201902579.

[26] D. Yang, X. Zhou, R. Yang, Z. Yang, W. Yu, X. Wang, C. Li, S. F. Liu, R. P. H. Chang, Surface optimization to eliminate hysteresis for record efficiency planar perovskite solar cells, *Energy & Environmental Science*, 2016, **9**, 3071-3078, doi: 10.1039/c6ee02139e.

[27] Y.-C. Wang, J. Chang, L. Zhu, X. Li, C. Song, J. Fang, Electron-transport-layer-assisted crystallization of perovskite films for high-efficiency planar heterojunction solar cells, *Advanced Functional Materials*, 2018, **28**, 1706317, doi: 10.1002/adfm.201706317.

[28] Y. Cao, G. Yang, A nanoscale temperature-dependent heterogeneous nucleation theory, *Journal of Applied Physics*, 2015, **117**, 224303, doi: 10.1063/1.4922415.

[29] K. Choi, J. Lee, H. I. Kim, C. W. Park, G.-W. Kim, H. Choi, S. Park, S. A. Park, T. Park, Thermally stable, planar hybrid perovskite solar cells with high efficiency, *Energy & Environmental Science*, 2018, **11**, 3238-3247, doi: 10.1039/c8ee02242a.

[30] P. Zhang, F. Yang, M. A. Kamarudin, C. H. Ng, G. Kapil, T. Ma, S. Hayase, Performance enhancement of mesoporous TiO_2-based perovskite solar cells by SbI_3 interfacial modification layer, *ACS Applied Materials & Interfaces*, 2018, **10**, 29630-29637, doi: 10.1021/acsami.8b10062.

[31] T. Bu, J. Li, F. Zheng, W. Chen, X. Wen, Z. Ku, Y. Peng, J. Zhong, Y.-B. Cheng, F. Huang, Universal passivation strategy to slot-Die printed SnO_2 for hysteresis-free efficient flexible perovskite solar module, *Nature Communications*, 2018, **9**, 4609, doi: 10.1038/s41467-018-07099-9.

[32] X. Zhu, Z. Xu, S. Zuo, J. Feng, Z. Wang, X. Zhang, K. Zhao, J. Zhang, H. Liu, S. Priya, S. F. Liu, D. Yang, Vapor-fumigation for record efficiency two-dimensional perovskite solar cells with superior stability, *Energy & Environmental Science*, 2018, **11**, 3349-3357, doi: 10.1039/c8ee02284d.

[33] S. Yang, Q. Han, L. Wang, Y. Zhou, F. Yu, C. Li, X. Cai, L. Gao, C. Zhang, T. Ma, Over 23% power conversion efficiency of planar perovskite solar cells via bulk heterojunction design, *Chemical Engineering Journal*, 2021, **426**, 131838, doi: 10.1016/j.cej.2021.131838.

[34] Z. Tang, S. Tanaka, S. Ito, S. Ikeda, K. Taguchi, T. Minemoto, Investigating relation of photovoltaic factors with properties of perovskite films based on various solvents, Nano Energy, 2016, **21**, 51-61, doi: 10.1016/j.nanoen.2015.12.013.

[35] Z. Liu, J. Hu, H. Jiao, L. Li, G. Zheng, Y. Chen, Y. Huang, Q. Zhang, C. Shen, Q. Chen, H. Zhou, Chemical reduction of intrinsic defects in thicker heterojunction planar perovskite solar cells, *Advanced Materials*, 2017, **29**, 1606774, doi: 10.1002/adma.201606774.

[36] Y. Wang, M. I. Dar, L. K. Ono, T. Zhang, M. Kan, Y. Li, L. Zhang, X. Wang, Y. Yang, X. Gao, Y. Qi, M. Grätzel, Y. Zhao, Thermodynamically stabilized β-CsPbI 3-based perovskite solar cells with efficiencies >18%, *Science*, 2019, **365**, 591-595, doi: 10.1126/science.aav8680.

[37] G.-J A. H. Wetzelaer, M. Scheepers, A. M. Sempere, C. Momblona, J. Ávila, H. J. Bolink, Trap-assisted non-radiative recombination in organic-inorganic perovskite solar cells, *Advanced Materials*, 2015, **27**, 1837-1841, doi: 10.1002/adma.201405372.

[38] T. Bu, J. Li, F. Zheng, W. Chen, X. Wen, Z. Ku, Y. Peng, J. Zhong, Y.-B. Cheng, F. Huang, Universal passivation strategy to slot-Die printed SnO_2 for hysteresis-free efficient flexible perovskite solar module, *Nature Communications*, 2018, **9**, 4609, doi: 10.1038/s41467-018-07099-9.

[39] M. Wei, K. Xiao, G. Walters, R. Lin, Y. Zhao, M. I. Saidaminov, P. Todorović, A. Johnston, Z. Huang, H. Chen, A. Li, J. Zhu, Z. Yang, Y.-K. Wang, A. H. Proppe, S. O. Kelley, Y. Hou, O. Voznyy, H. Tan, E. H. Sargent, Combining efficiency and stability in mixed tin-lead perovskite solar cells by capping grains with an ultrathin 2D layer, *Advanced Materials*, 2020, **32**, 1907058, doi: 10.1002/adma.201907058.

[40] Y. Zhao, P. Zhu, M. Wang, S. Huang, Z. Zhao, S. Tan, T.-H. Han, J.-W. Lee, T. Huang, R. Wang, J. Xue, D. Meng, Y. Huang, J. Marian, J. Zhu, Y. Yang, A polymerization-assisted grain growth strategy for efficient and stable perovskite solar cells, *Advanced Materials*, 2020, **32**, 1907769, doi: 10.1002/adma.201907769.

Author Information

Putao Zhang *received his Ph.D. from the Graduate school of life science and systems engineering, Kyushu Institute of Technology in 2019. His research interests focus on nano materials and optoelectronic devices. He works at Henan University since 2019 to now. His current research interests include the fundamental electronic processes involved in charge photogeneration and device fabrication of mixed cation perovskite semiconductors.*